Faculty of Engineering and the Built Environment
Department of Electrical Engineering

Hopping Control of a Single Leg Robot

Prepared for Dr. Amir Patel.
Submitted to the Department of Electrical Engineering
at the University of Cape Town in partial fulfilment of the academic requirements
for a Bachelor of Science degree in Mechatronics.

Benjamin Scholtz

October 23, 2016

Keywords: impedance control, virtual model, force control, mechatronics

To my dearest...

Declaration

1. I know that plagiarism is wrong. Plagiarism is to use another's work and pretend that it is one's own.
2. I have used the IEEE convention for citation and referencing. Each contribution to, and quotation in, this final year project report from the work(s) of other people, has been attributed and has been cited and referenced.
3. This final year project report is my own work.
4. I have not allowed, and will not allow, anyone to copy my work with the intention of passing it off as their own work or part thereof.

Name: Benjamin Scholtz
Signature: _____
Date: October 23, 2016

Abstract

Acknowledgements

Amir Patel Callen Fisher Craig Burden Gareth Callanan Roberto Aldera

Ben Bingham Luke Bell

Terms of Reference

Description

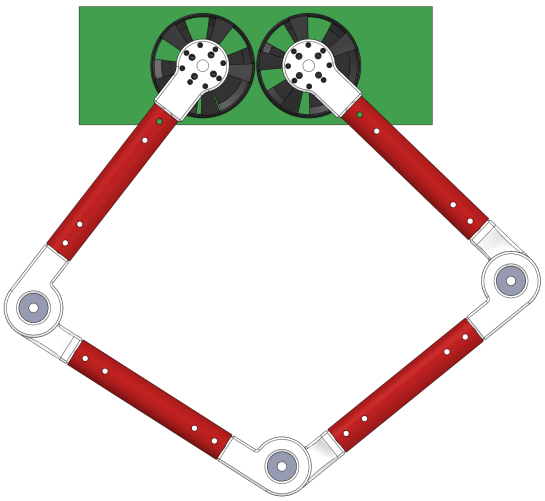

Figure 1: Version 1 of Baleka leg platform (Ben Bingham, 2016).

The Mechatronics Lab has recently developed a single leg, direct drive robot, Baleka, to investigate modelling and control of rapid accelerations. This project will involve the design of a control system to perform stable hopping with the robot. Various controller algorithms will be investigated and compared (eg. PID, MPC, etc.). The project will also involve developing a test rig for the robot.

Deliverables

- Mathematical model of the hopping robot must be developed in Simulink/Matlab
- Hopping controller design

- Mechanical design of the test rig
- Experimental testing of the robot

Skills/Requirements

- Mathematical Modelling
- Mechatronics Design
- Control Systems
- Embedded Systems
- Strong Practical and Mathematical skills required

ELO3: Engineering Design

Perform creative, procedural and non-procedural design and synthesis of components, systems, engineering works, products or processes.

The student is expected to design:

- Robot feedback control system
- Rig for testing of hopping motion

Area of Research

- Bio-inspired robotics
- Control systems

Extra Information

http://ieeexplore.ieee.org/xpls/abs_all.jsp?arnumber=5648972

http://kodlab.seas.upenn.edu/uploads/Avik/compositionTR_sc.pdf

Contents

List of Figures

List of Tables

List of Source Codes

1 Introduction

> *"Begin at the beginning," the King said, gravely, "and go on till you come to an end; then stop."*
>
> — Lewis Carroll, *Alice in Wonderland*

With a hop, skip, and a jump – the journey begins!

1.1 Background

1.2 Objectives of the Study

1.2.1 Problems to be Investigated

1.2.2 Research Questions

1.2.3 Purpose of the Study

1.3 Scope and Limitations

1.4 Plan of Development

2 Literature Review

2.1 Introduction

Bio-inspired robots have fascinated humans since the Greek mathematician, Archytas of Tarentum, built the first true mechanical robot, where a robot is some device performing an automated mechanical task. His mechanical steam powered bird was just the start.[**?**]

Would be engineers take their inspiration from popular culture with The Iron Giant and B.E.N. fresh in mind. The Rising Sun included robots developed by Marc Raibert, founder of the CMU (now MIT) Leg Laboratory, who pioneered self-balancing dynamic control of hopping robots.

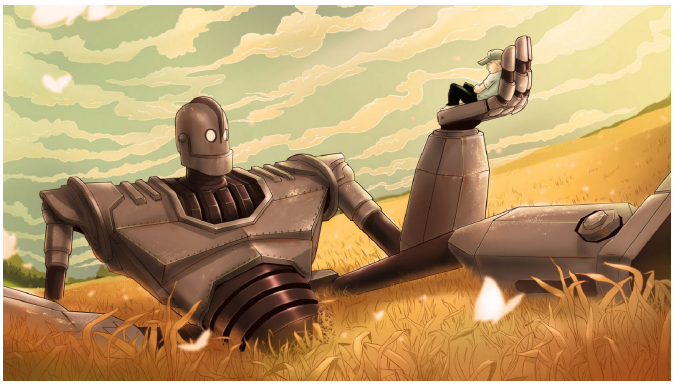

(a) The Iron Giant (1999).

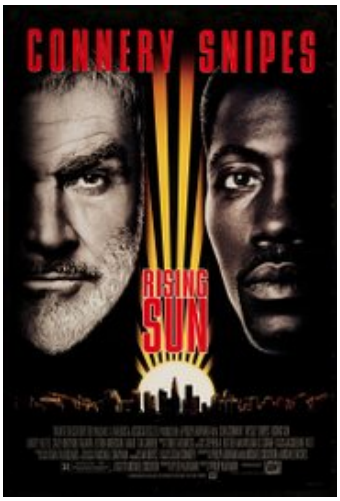

(b) Rising Sun (1993).

(c) Treasure Planet (2002).

Figure 2.1: Humanoid robots in popular culture.

2.2 State of the Art

2.2.1 Monoped Robots

2.2.2 Biped Robots

2.2.3 Quadruped Robots

2.2.4 Bio-inspired Legged Robotics

2.2.5 Humanoid Robots

2.2.6 Closed Kinematic Chain Leg

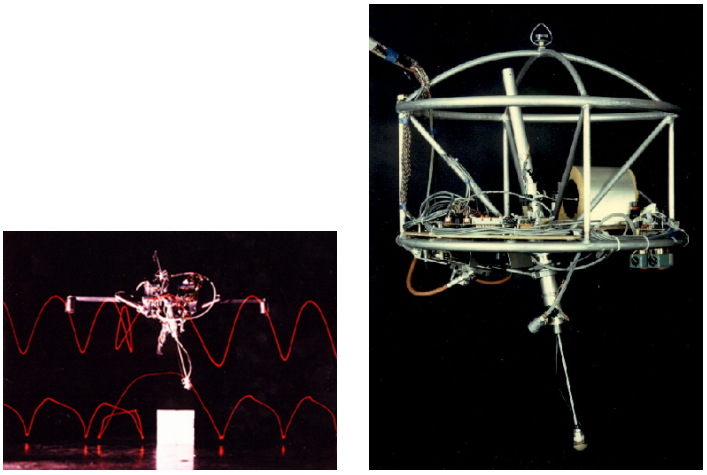

(a) Planar One-Leg Hopper - MIT Leg Laboratory (1980-1982).

(b) 3D One-Leg Hopper - MIT Leg Laboratory (1983-1984).

Figure 2.2: Monoped robots.

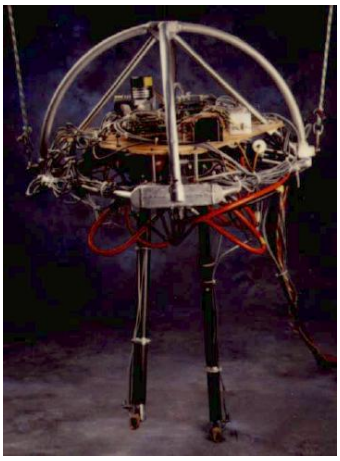

Figure 2.3: 3D Biped - MIT Leg Laboratory (1989-1995).

(a) Quadruped - MIT Leg Laboratory (1984-1987).

(b) GOAT 3-DOF Leg Topology - (Kalouche, 2016).

Figure 2.4: Quadruped robots.

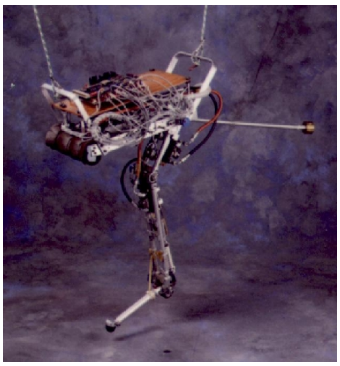

(a) Uniroo - MIT Leg Laboratory (1991-1993).

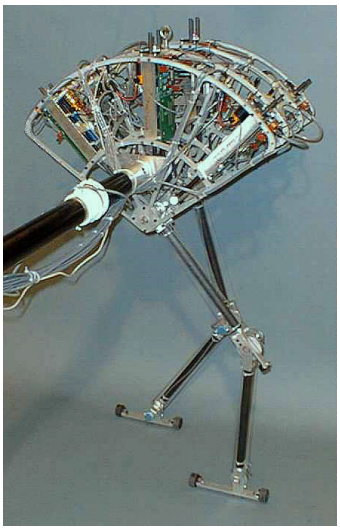

(b) Spring Flamingo - MIT Leg Laboratory (1996-2000).

Figure 2.5: Bio-inspired legged robots.

Figure 2.6: Atlas Humanoid Robot - Boston Dynamics (2013).

Figure 2.7: Closed Kinematic Chain Leg using Raibert's Scissor Algorithm (Duperret, Koditschek, 2016).[?]

2.3 Legged Locomotion in Nature

2.4 Raibert Control

2.4.1 Raibert's Scissor Algorithm

2.4.2 Phases of Motion

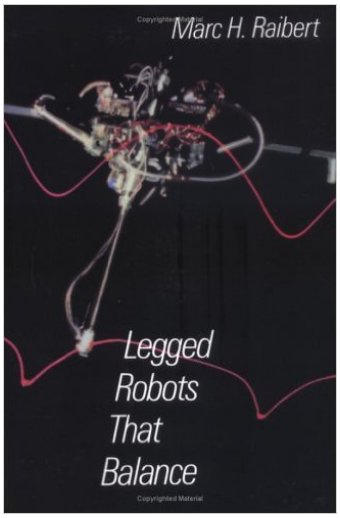

(a) Legged Robots That Balance - Marc H. Raibert (1986).

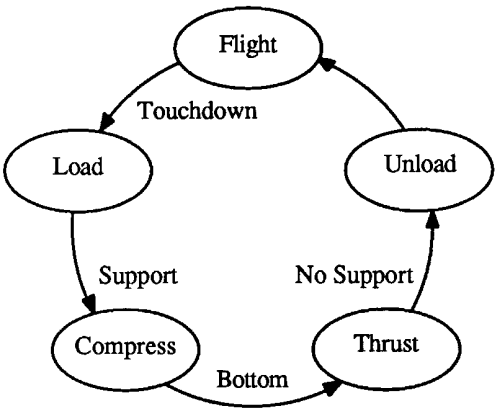

(b) Raibert control state machine.

Figure 2.8: Legged Robots That Balance cover page and exert.[?]

2.5 Applications in Industry

2.5.1 Soft-robotics

Factories safe human robot interaction Handling of compliant products (farming, manufacturing)

[?]

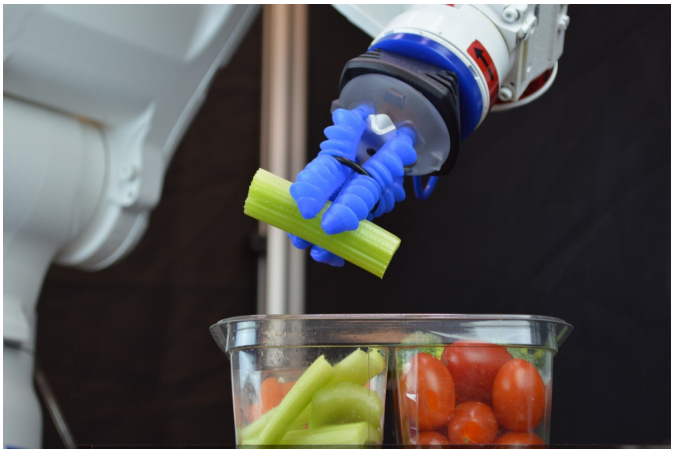

Figure 2.9: Compliant soft robotic handling (Forbes, 2016).

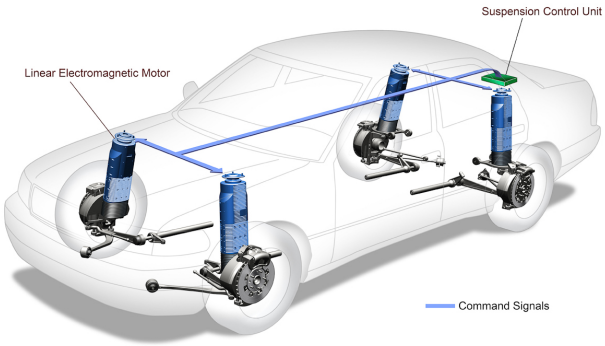

Figure 2.10: Bose Active Suspension (Bose Corporation, 1980s)[**?**].

2.5.2 Bose Active Suspension

2.5.3 Dynamic Stability vs Static Stability

2.5.4 Phases of Motion

2.5.5 Leg Stance Control

2.6 Force Control

3 Project Plan and Methodology

4 Theory Development

4.1 General Co-ordinates

5 System Modelling and Simulation

6 Leg Design and Construction

6.1 Original Leg Design

6.1.1 Leg Hip

The original leg 'hip' was designed by Ben Bingham in 2016 in completion of his undergraduate vacation work as seen in fig. 6.1.

The 'hip' was constructed of 6 mm perspex sheet in a box design with metal L connectors to join the sheets securely. The design of the 'hip' allowed the motor drivers as well as the microcontroller to be mounted on one leg, with space provided for an extra leg for future two-legged movement.

6.1.2 Leg Guide

The guiding system consisted of two parallel steel rods with ball bearings mounted on the 'hip'.

6.1.3 Problems with Design

The leg mounting plate went through three design iterations after the original 'hip' design before the final design was created, as seen in fig. 6.5c.

The original 'hip' design had the following mechanical design flaws:

1. The 6 mm perspex box construction with on-board microncontroller and motor drivers is too heavy for efficient jumping action when compared to similar designs like [**?**] (1.3 kg), [**?**] (2.5 kg), [**?**] (4.2 kg) where there is a high leg torque to mass ratio.
2. The ball bearings are particularly heavy.

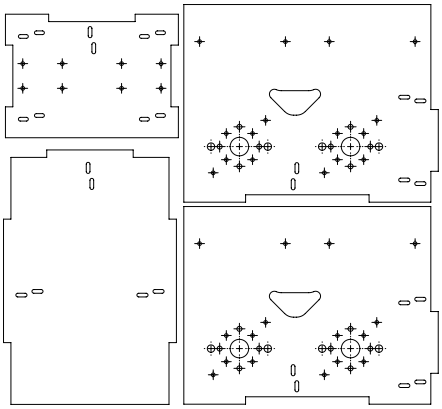

Figure 6.1: Original 'hip' design by Ben Bingham, 2016.

3. The mounting of the leg guide places a significant torque in all three cartesian coordinates being off-center from the center of mass.
4. The design of the leg guide requires the two steel rods to be perfectly parallel to remove resistance to movement, which is difficult to achieve practically.

These problems were accounted for by replacing the original 'hip' with a rigid aluminium mounting plate with off-board microcontroller and motor drivers. The leg guide consisting of parallel steel rods and ball bearings was replaced with a linear guide as seen in fig. 6.11.

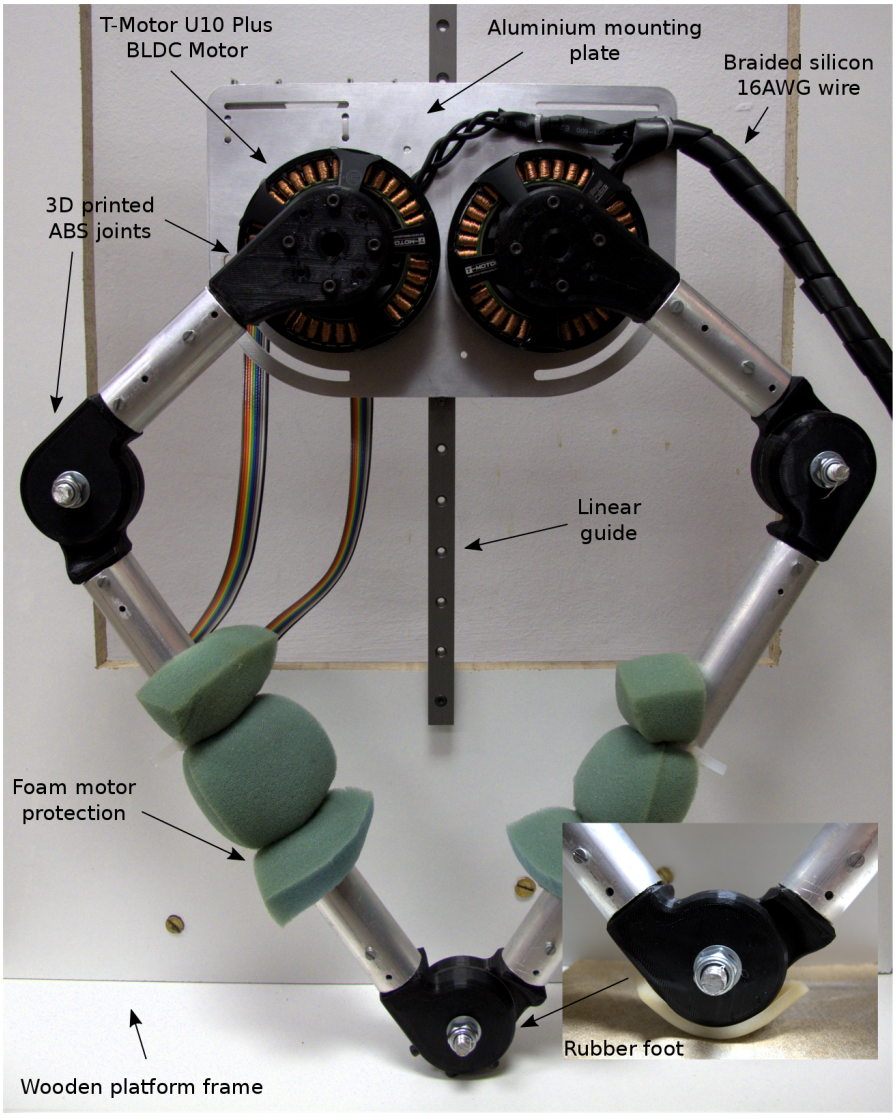

Figure 6.2: Final leg design mounted to platform and linear guide: front.

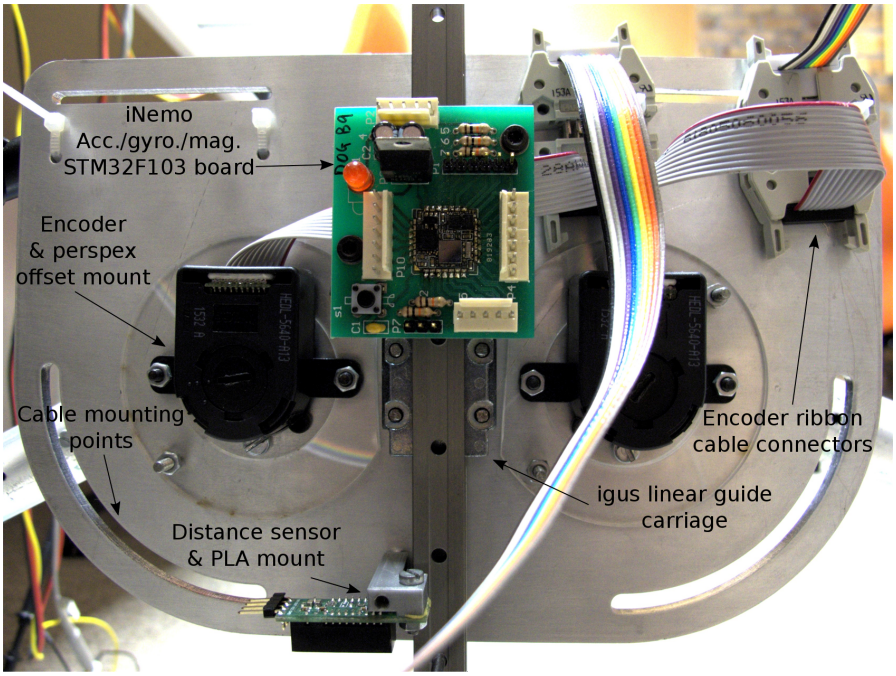

Figure 6.3: Final leg design mounted to platform and linear guide: back.

6.2 Geometry

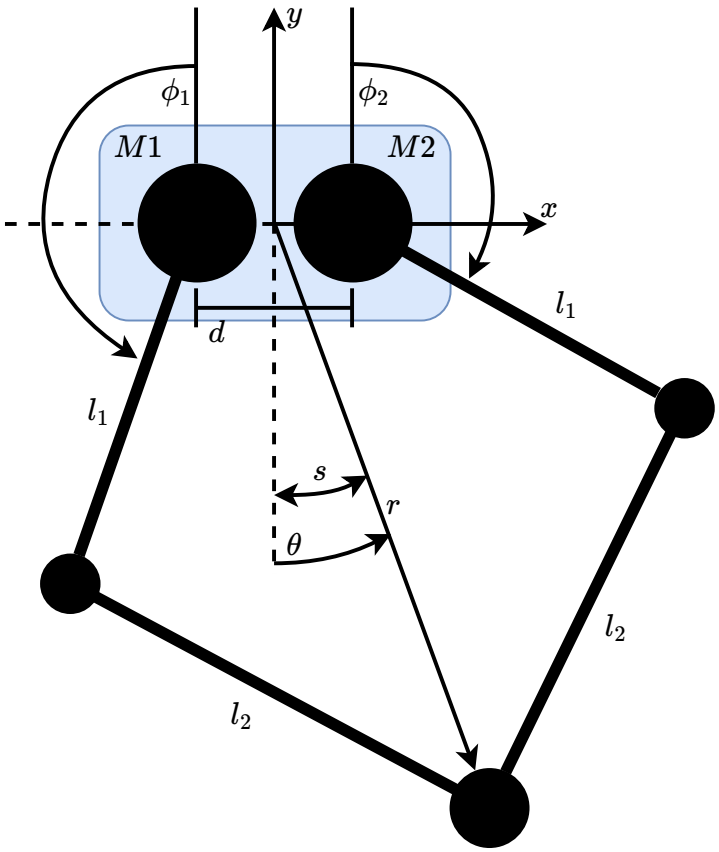

Figure 6.4: Geometric view of leg.

6.3 Mechanics and Construction

6.3.1 Alumnium Mounting Plate Design

6.3.2 Leg Linkage and Foot Design

The 4-bar linkage design of the leg was originally constructed by Ben Bingham in 2016 for completion of his undergraduate engineering vacation work in the mechatronics lab. The leg was constructed as follows:

- Three sets of rotational joints make up the linkage system. The joints were 3D printed using ABS plastic and used 3 mm screws to connect to the aluminium leg sections.
- 8 mm loctite nut, bolt and washer combinations connected the joint components with perspex discs to reduce friction between the joints.
- The aluminium leg sections were constructed of 25 mm diameter tubing to form a leg of 0.15 m and 0.3 m sections including the joints.

6.3.3 Linear Guide

6.3.4 CAD Robotic Leg Assembly

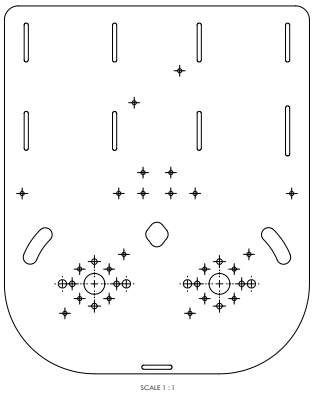

(a) CAD mounting plate V1.

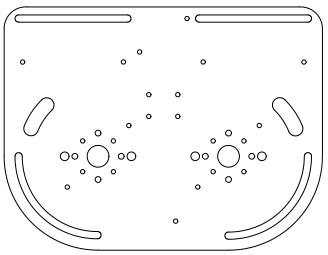

(b) CAD mounting plate V3.1.3.

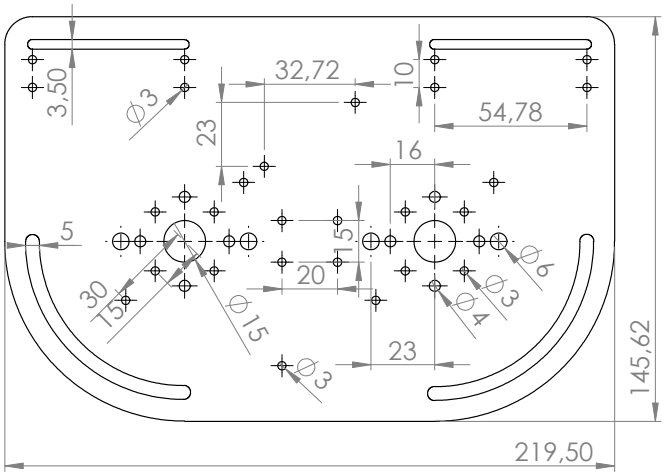

(c) CAD mounting plate final design.

Figure 6.5: Leg mounting plate iterations.

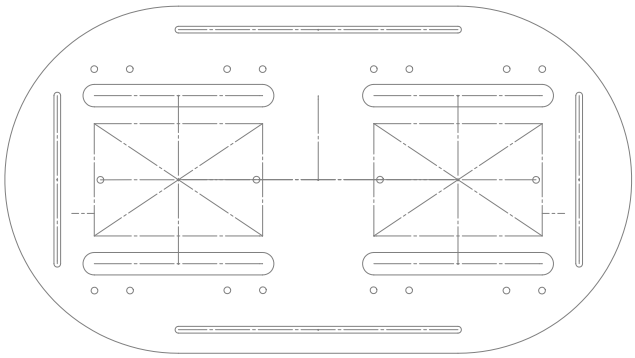

Figure 6.6: Motor driver interface mounting plate.

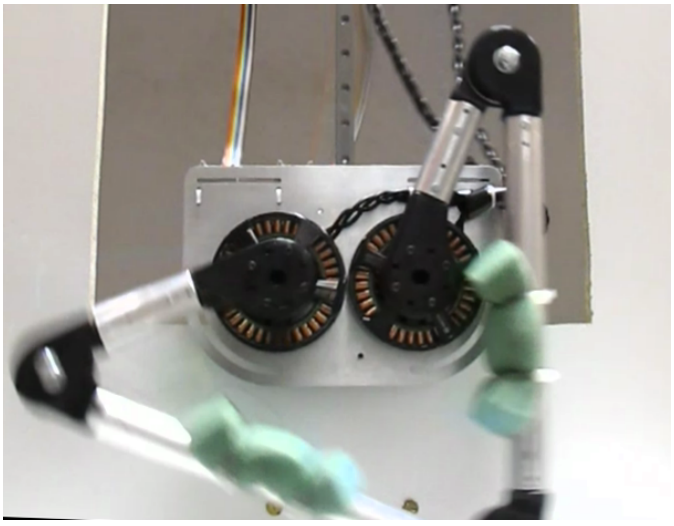

Figure 6.7: Leg foot lateral slipping.

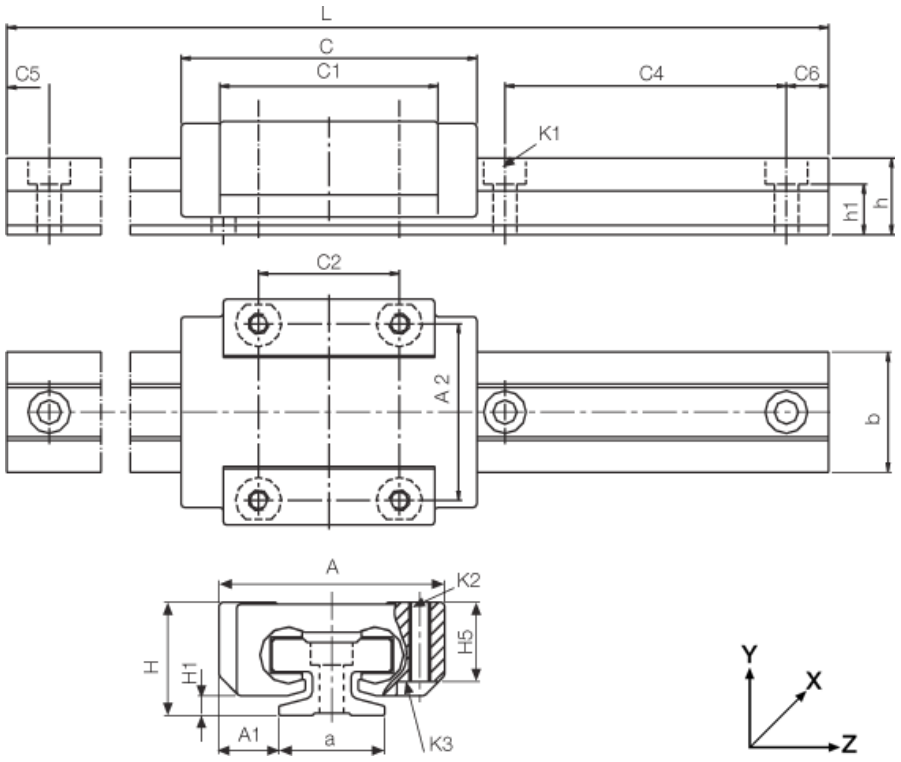

Figure 6.8: igus DryLin T - Low-profile linear guide.

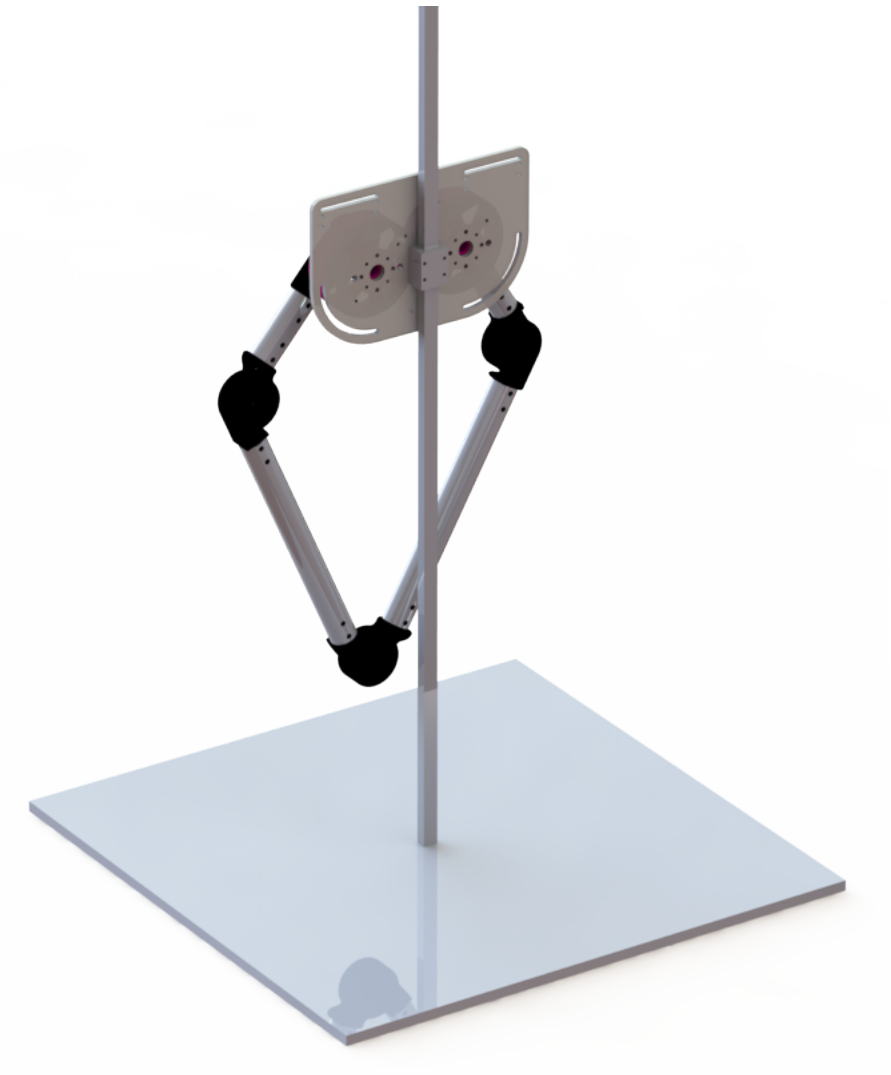

Figure 6.9: Linear guide mounted leg model (CAD Solidworks assembly).

6.4 Mass Distribution

Servo drive mounting card = 50.7g Servo drive = 123.9g T-Motor U10 Plus = 500g

Savings = 349.2g

Complete leg = 2.2kg Leg = 0.5kg Plate = 0.7kg Motors = 1kg

The center of mass (COM) moves negligibly with the foot position. To calculate a COM for placement of the linear guide mount and iNemo, a intermediate radial foot position of $0.25m$ was chosen - this position set-point was used for compliant landing and launch sequences. ...

...

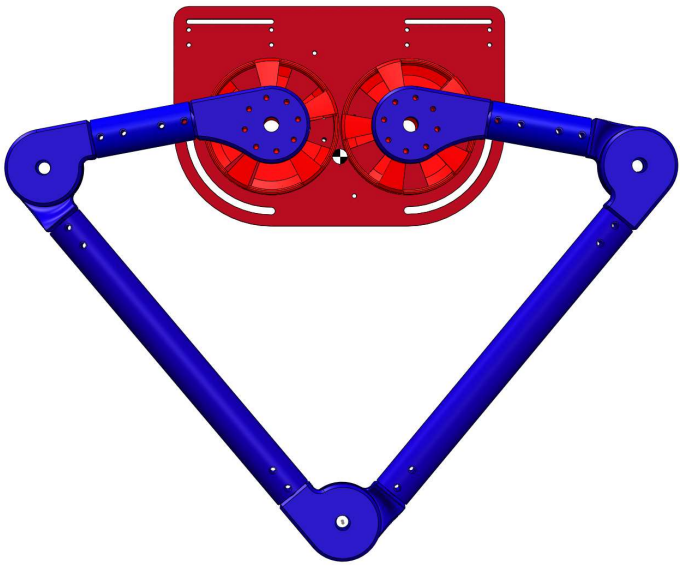

(a) Mass distribution graphic.

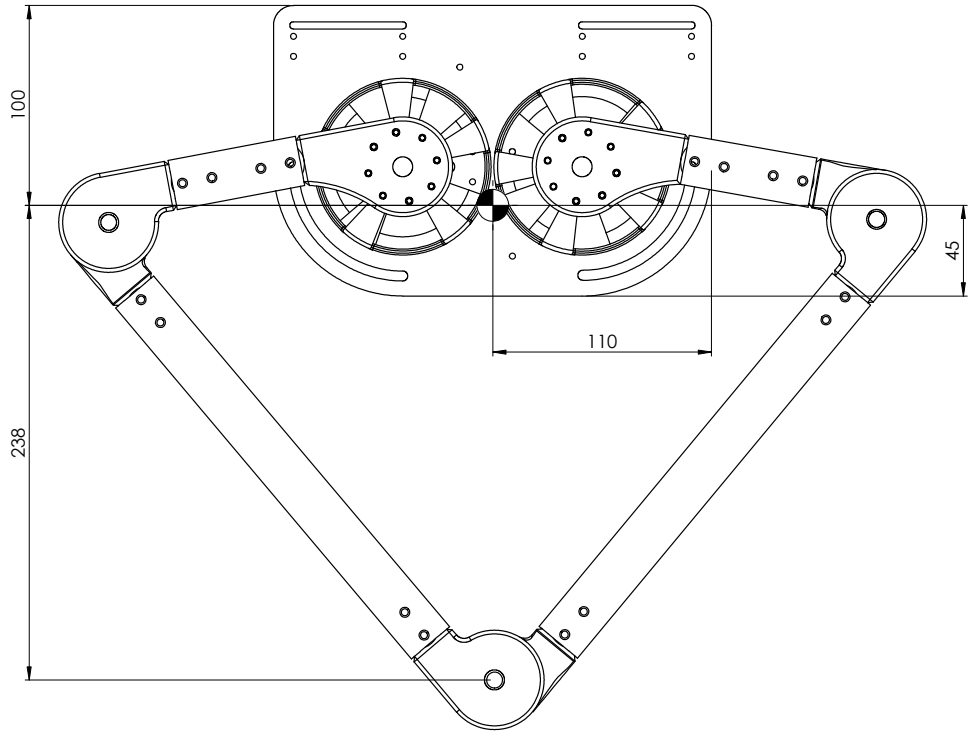

(b) Center of mass of leg assembly.

Figure 6.10: Mass distribution of leg assembly.

Colour legend	Component	No.	Mass (g)
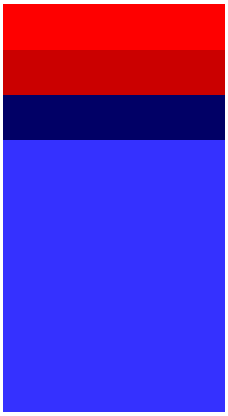	T-Motor U10 Plus	2	424.56
	Mounting Plate	1	378.86
	Linear Guide Carriage	1	100.37
	ABS Motor Joint	2	50.55
	Long Linkage	2	46.40
	Joint	5	39.83
	Foot Joint	1	39.63
	Short Linkage	2	12.81
	Washer Bearing	3	2.41
Total:			**1793.88**

Table 6.1: Solidworks leg assembly mass distribution.

6.5 Electronics and Communication

6.5.1 Accelerometer and Gyroscope

6.5.2 Distance Sensor

6.5.3 Microcontroller

6.5.4 Shielding

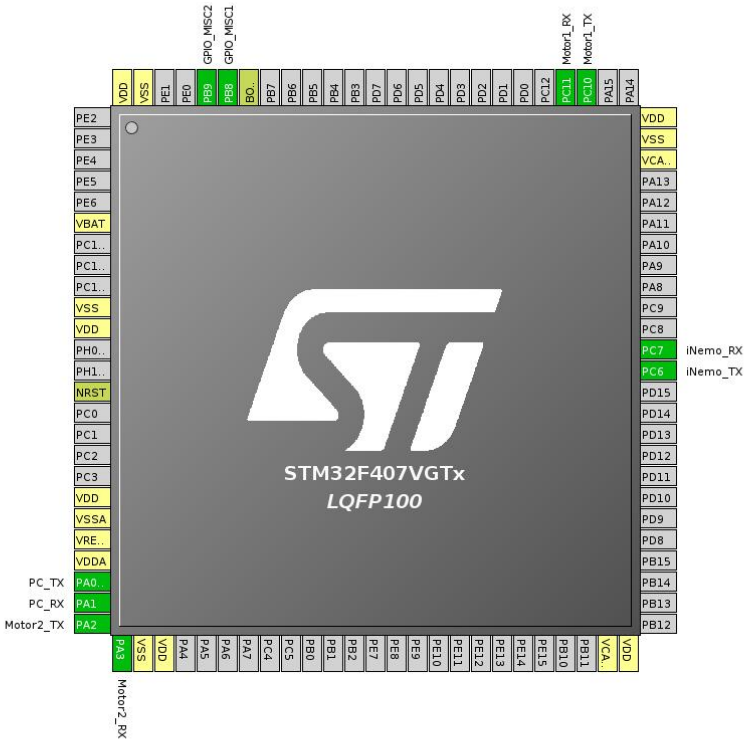

Figure 6.11: STM32F4 microcontroller peripheral configuration.

6.6 Motors and Drivers

6.6.1 Driver Selection

6.6.2 Motor Selection

In the study by [**?**] various COTS (commercial off the shelf) motors were compared using the thermal specific torque as a performance measure. The T-Motor U10 Plus was found to have the highest thermal specific torque at $0.42\frac{Nm}{kgC^o}$ at $r_{gap} = 40mm$ [**?**]. When compared to the custom made MIT Cheetah motors at $0.71\frac{Nm}{kgC^o}$ at $r_{gap} = 49mm$ found in [**?**] they perform favourably.

6.6.3 Motor Model Calculations

Experimental Calculation of K_t and K_e

The motor torque constant, K_t, was calculated using the torque current relation $\tau = K_t I$. The leg was modelled as a virtual spring-damper system, as seen in fig. 10.1.

The spring constant, K_{s1}, was set to $200\ [N/m]$, and the damping and torsional spring-damping constants were set to zero. K_t was tuned until the theoretical foot force matched the practical foot force measured via a scale. The leg was fixed at a set height imposing a radial offset on the virtual spring-damper system.

For a spring constant of $200\ [N/m]$ and a radial offset of $0.15\ m$ a theoretical foot force of $K_{s1}\Delta r = 30\ N$ was expected. A mass of approximately $3\ kg$ was measured with $K_t = 0.08\ [Nm/A]$ set in the virtual leg model controller, resulting in a foot force of $3\ kg \times 9.81\ m/s^2 = 29.43\ [N]$.

The study in [**?**], using the same T-Motor U10 Plus motors, calculated a torque constant of $K_t = 0.072\ [Nm/A]$. This confirms the experimental results obtained above.

For an ideal motor at a constant operating point, K_e will equal K_t, as shown in eq. (6.1).

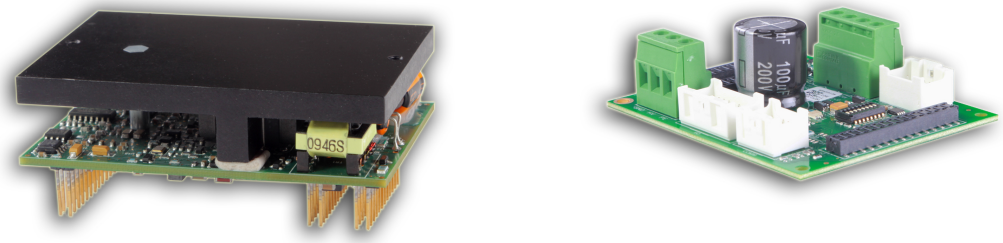

(a) AMC DigiFlex Performance Servo Drive.

(b) AMC DigiFlex Performance Servo Drive mounting card.

Figure 6.12: AMC Servo Drive and Mounting Card.

Figure 6.13: T-Motor U10 Plus Brushless DC Motor.

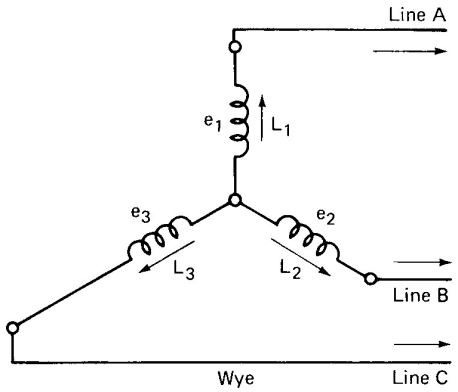

Figure 6.14: WYE connected BLDC motor windings.

$$
\begin{aligned}
&V_t = K_e\omega_m + IR_m \\
&\tau_m = K_tI \\
&P_{elec.} = V_tI = K_e\omega_mI + I^2R \\
&P_{mech.} = \tau_m\omega_m = K_tI\omega_m \\
&P_{loss.} = I^2R_m \\
&P_{elec.} = P_{mech.} + P_{loss.} \\
&\therefore K_e\ [V/rad/s] = K_t\ [Nm/A] = 0.08
\end{aligned}
\tag{6.1}
$$

Calculation of R_m and L_m

The resistance and inductance of the 3 phase windings of the motor were calculated using a lab multimeter to be $R_m = 47.5\ m\Omega$ and $L_m = 35\ \mu H$ respectively.

Brushless DC motor windings are usually connected in WYE formation, as seen in **??**. This means the measured values for resistance and inductance were line-to-line values and had to be divided by two to get the per phase values above.

Calculation of J_m

In order to calculate the moment of inertia of the motor, J_m, the ratio of acceleration torque to acceleration to steady state needs to be found. By commanding a DC equivalent current input of $1\ A$ and measuring the time taken to reach a steady state velocity,

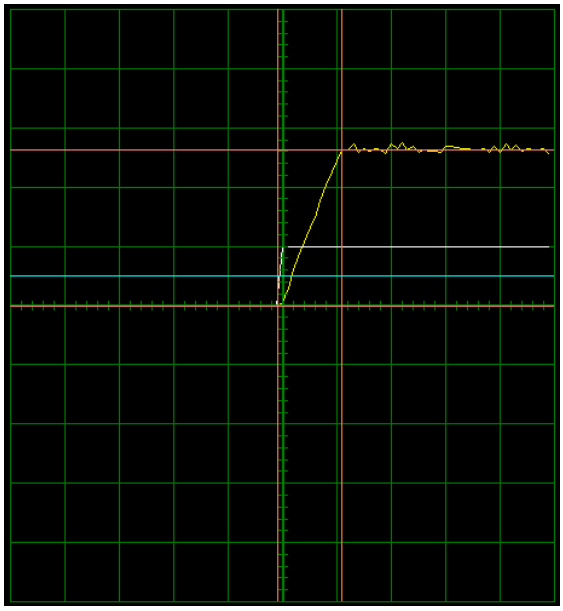

Figure 6.15: Velocity vs. time plot for 1A equivalent DC command.
(500 rpm; 500 ms/div)

eq. (6.2) can be used to calculate J_m. The velocity vs. time plot used can be seen in fig. 6.15.

$$\begin{aligned} J_m &= \frac{T_{acc.}[N/m]}{a[m/s^2]} \\ &= \frac{IK_t}{a} \\ &= \frac{IK_t}{\frac{\Delta v}{\Delta t}}\ [kg/m^2] \end{aligned} \tag{6.2}$$

where $I = 1\ A$, $K_t = 0.08\ Nm/A$, $\Delta v = 1313.906 \times \frac{2\pi}{60}\ rad/s$ and $\Delta t = 588.889 \times 10^{-3}\ s$. This results in a motor moment of inertia of $J_m = 3.424 \times 10^{-4}\ [kg/m^2]$.

Calculation of B_m

The motor damping or viscous friction, B_m, was assumed to be negligible. Brushless DC motors have near zero damping and will have little effect on the simulated motor model.

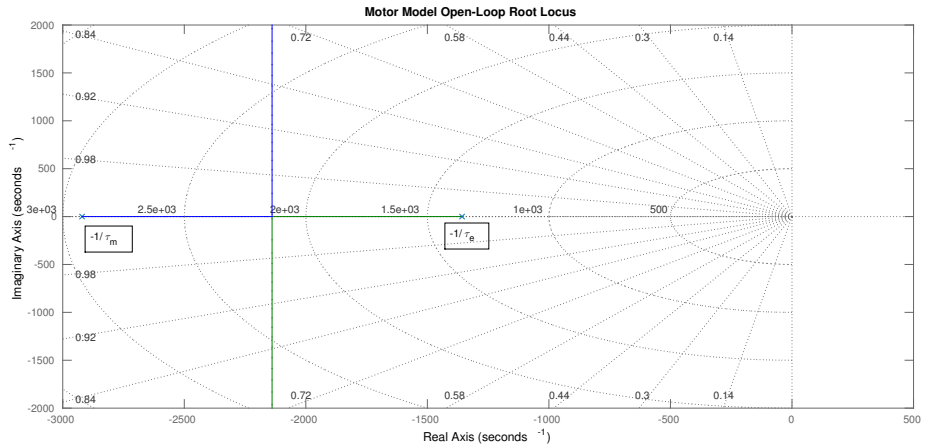

Figure 6.16: Motor model open loop root-locus plot.

Calculation of τ_e and τ_m

The electrical and mechanical time constants of the motor, τ_e and τ_m respectively, can be used to plot a root-locus plot with poles at $-\tau_e$ and $-\tau_m$ as can be seen in **??**. This is useful when designing a current controller for the system. τ_e and τ_m can be calculated using eq. (6.3).

$$\begin{aligned} K_m &= \frac{1}{B_m} \\ \tau_m &= \frac{J_m}{B_m} \\ K_e &= \frac{1}{R_m} \\ \tau_e &= \frac{L_m}{R_m} \end{aligned} \tag{6.3}$$

From eq. (6.3) and using the previously calculated motor constants, $\tau_e = 7.368 \times 10^{-4}$ and $\tau_m = 3.424 \times 10^{-4}$. This is assuming a motor viscous friction of $B_m = 0$.

The resulting motor model open loop root-locus plot can be seen in fig. 6.16. As expected the system has only negative real roots and will be stable in open loop.

6.6.4 Driver Configuration

The AMC drivers allow extensive customisation. After the motor, encoder, and general communication control parameters are configured, the PID control loops of the drivers can be configured, as seen in fig. 6.17.

The motor drivers were initially configured with both on-board PID current and position control loops enabled. This allowed initial modelling of the motors, configuring of the motor encoders, and determining of the position limits (in counts). For control of the leg, the position control loop was finally implemented on the STM32F4 microcontroller, while using the existing current control loop of the motor drivers.

The AMC drivers were configured using the AMC Driveware configuration software, which provided an oscilloscope to measure the relevant motor responses as seen in figs. 6.15, 6.18 and 6.19.

Current Control Loop

By using a 1 A 120Hz square wave current command the current PI control loop was tuned, as seen in fig. 6.18. Initially both the proportional gain, K_p, and the integral gain, K_i, were set to zero. K_p was slowly increased until the final amplitude of the current output just started to overshoot. K_i was then set to minimize the steady state error.

Values of $K_p = 0.277$ and $K_i = 0.262$ were obtained. Both motors were found to operate optimally with the same PI gain values.

Position Control Loop

The on-board AMC motor driver control loop was set up to test the encoder configuration. The encoder and relevant position limits can be seen in subsection 6.6.5.

A 1Hz sinusoid was used to tune the PID control loop gains. Values of $K_p = 0.0005793$, $K_i = 0.0006052$ and $K_d = 2.769e - 9$ were found to achieve optimal set-point tracking as seen in fig. 6.19. The sinusoidal set-point can be seen in white and the position feedback in yellow. A 10-30 ms lag time can be seen due to the inertial load. This lag time causes a dead-band which should be considered when implementing a controller.

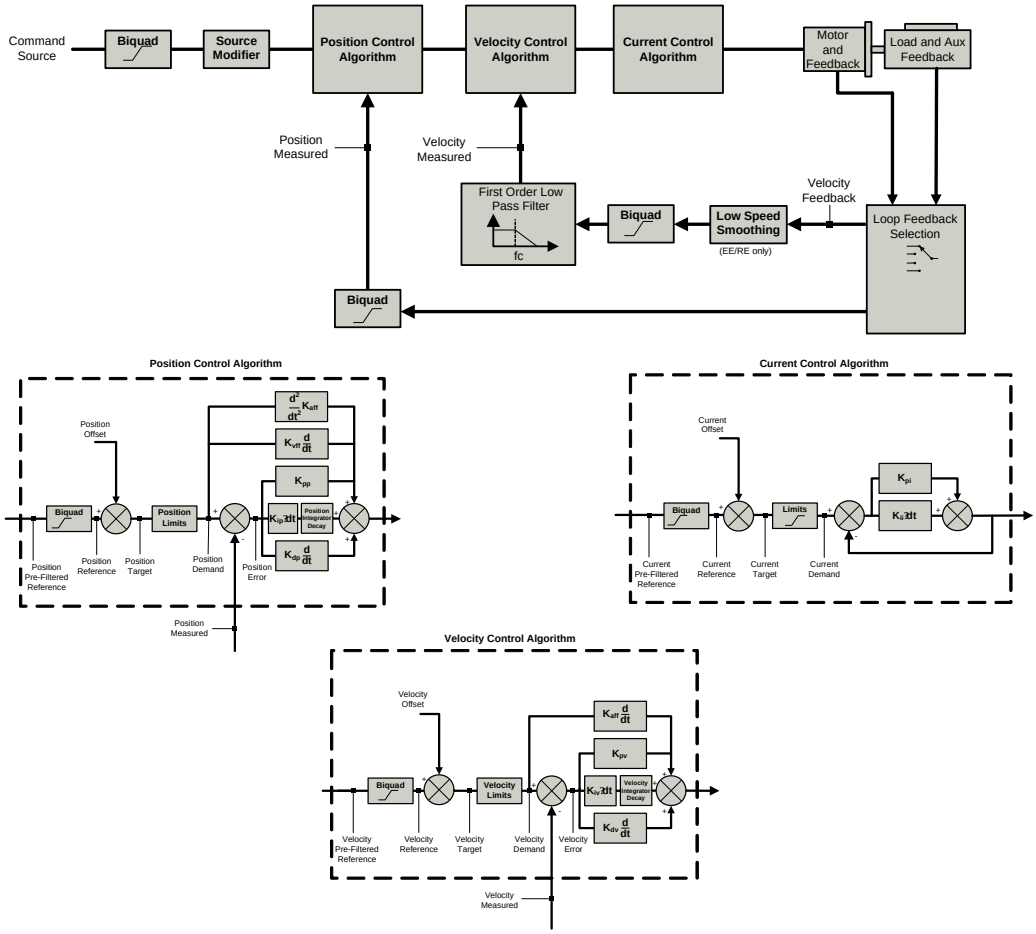

Figure 6.17: AMC DigiFlex Performance Servo Drive control loops (AMC, 2014).

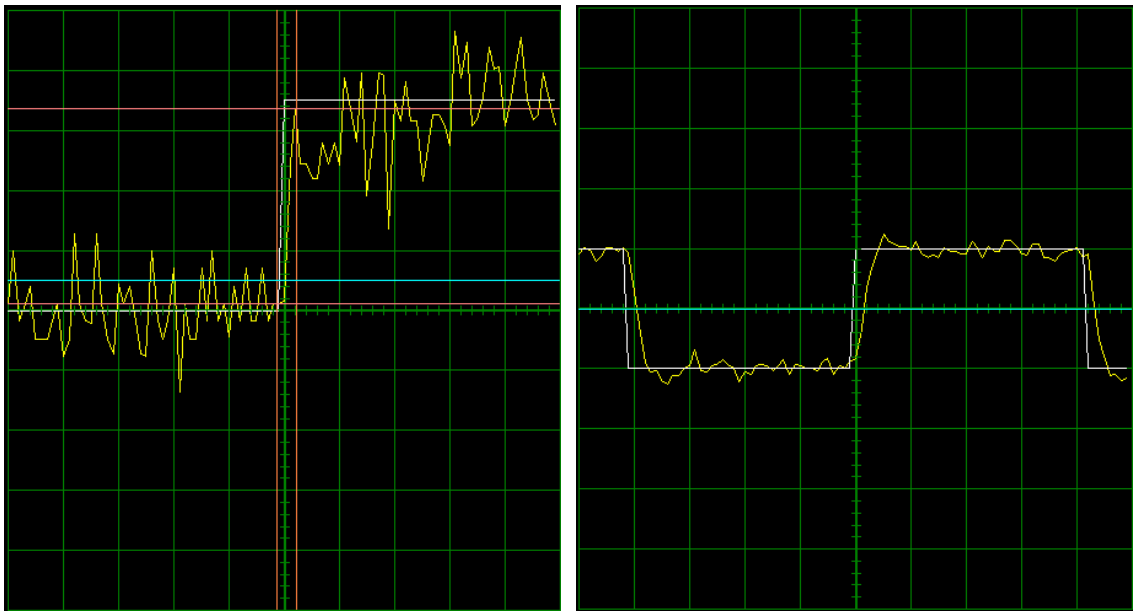

(a) Motor driver current loop pre-tuning.
(200 mA; 5 ms/div)

(b) Motor driver current loop tuning - 1A 120Hz square wave command.
(1 A; 1 ms/div)

Figure 6.18: Motor driver current loop tuning plots.

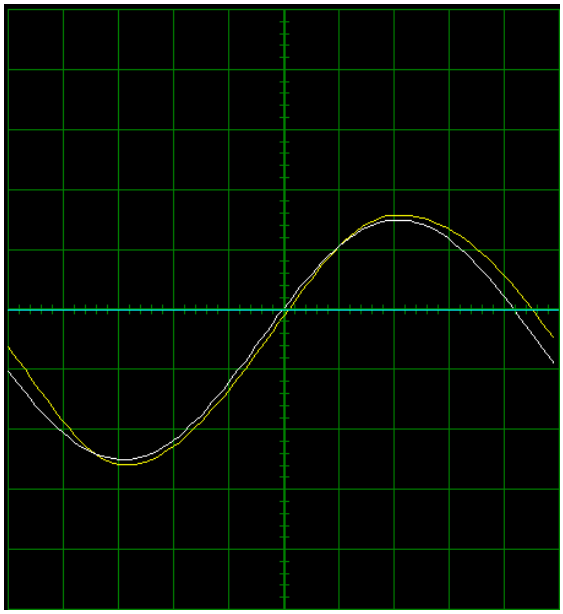

Figure 6.19: Motor driver position loop tuning - (-350:200) count 1Hz sinusoid command with 300 count offset.
(100 ct; 100 ms/div)

These tests were performed with the leg attached - the inertial load provided by the leg made PID control loop tuning possible, whereas without any inertial load the BLDC motors overshot their set-point.

6.6.5 Motor Encoders

6.6.6 Tuning and Optimisation

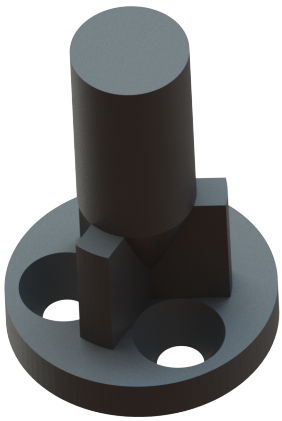

Figure 6.20: 3D printed PLA motor encoder shaft.

7 Communication Protocol

7.1 FreeRTOS

Ideally FreeRTOS tasks should operate with as much isolation as possible, with each task performing a specific function with different priority levels. In the case of a communication protocol, the overall task is inherently sequential so this leads to FreeRTOS being used in a sequential way with all tasks operating at real-time priority level.

FreeRTOS was chosen because of the following benefits:

1. Segmentation of code into specific tasks provides readable code for future users.
2. FreeRTOS task configuration provides a framework for future embedded robotic control systems as well as easily reconfigurable code.
3. Semaphores and queues lend themselves to sequential reception and processing of packets at predefined intervals very well.
4. Isolation of tasks provides easy debugging of communication issues.

7.1.1 Heartbeat Task

7.1.2 PC TX Task

7.1.3 PC RX Task

7.1.4 TX Motor Task

7.1.5 RX Motor Task

7.1.6 Controller Task

7.1.7 FreeRTOS Timing

The default 1000 Hz tick rate was overridden with a tick rate of 5000 Hz to enable more fine tuned packet timing and delays. The timing configuration can be seen in listing 1.

In order to achieve a control loop rate of 200 Hz, a sampling time of 5 ms or 25 ticks was used.

7.2 Packet Encoding and Decoding

SeqBits bits 2-5 switch case

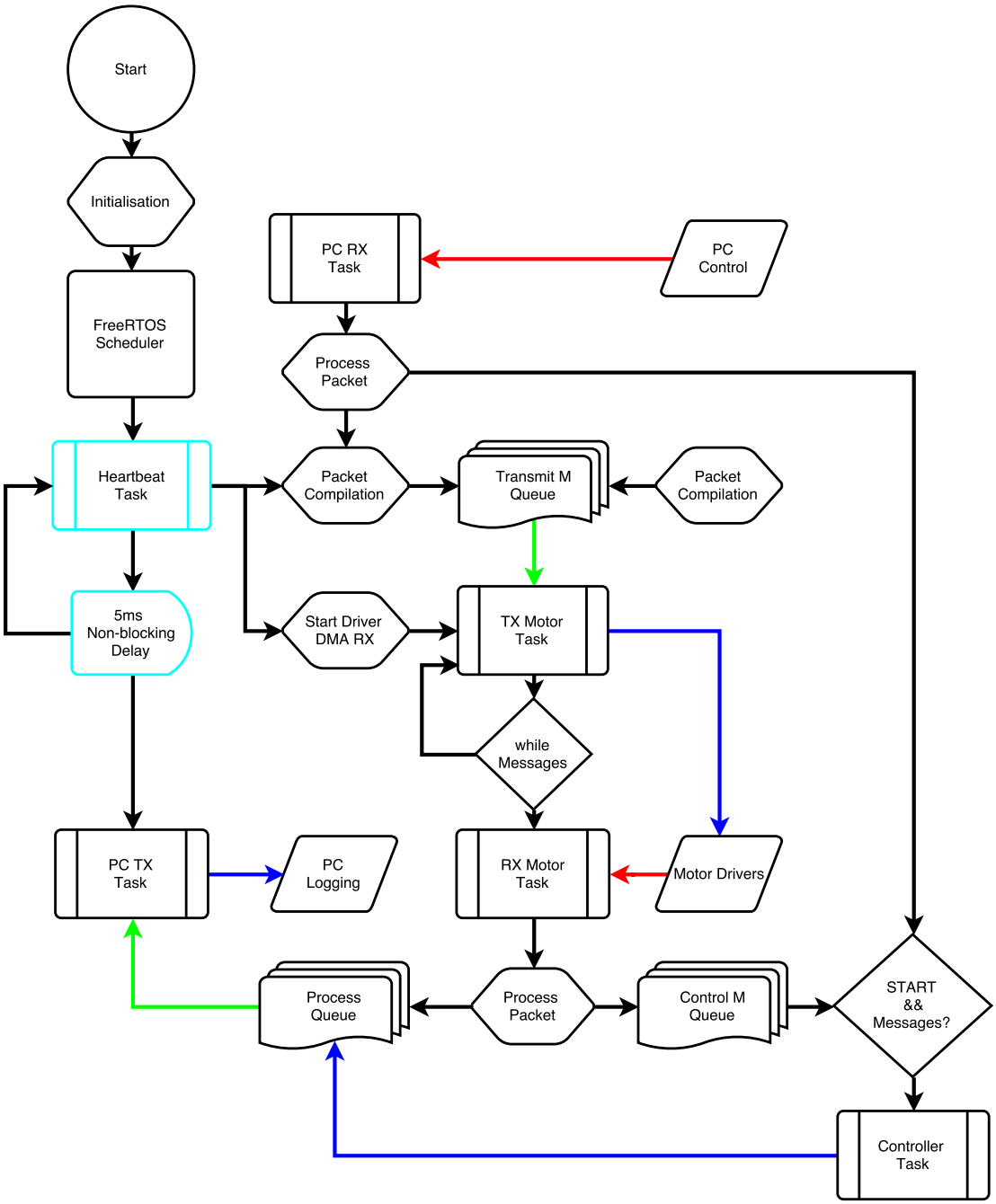

Figure 7.1: FreeRTOS communication protocol flow diagram.

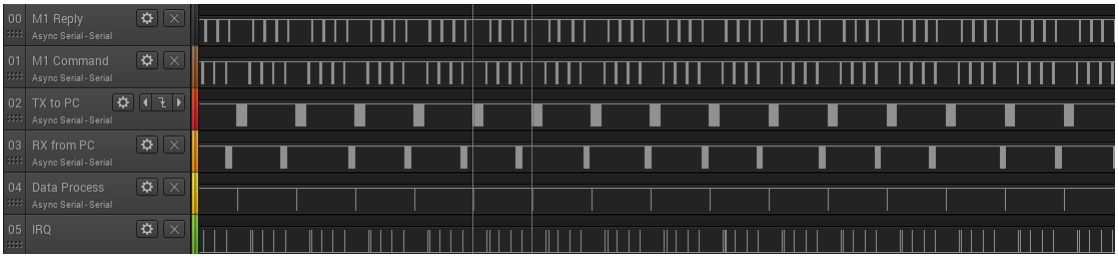

Figure 7.2: Communication protocol packet timing with 5 ms sampling rate.

Command	Index	Op-Code	TX CB	TX CRC1	RX CB
Kill Bridge	1	0001	0x06	0xCBB6	0x04
Write Enable	2	0010	0x0A	0x3624	0x08
Bridge Enable	3	0100	0x12	0x1AE0	0x10
Set Current	4	0011	0x0E	0xBF7B	0x0C
Read Current	5	1100	0x31	0x9772	0x32
Read Position	6	1111	0x3D	0xD310	0x3E
Read Velocity	7	0101	0x15	0x5EAF	0x16
Set Position	8	1010	0x2A	0x42C4	0x28

Table 7.1: Motor driver command protocol.

8 Graphic User Interface

8.1 Serial Communication

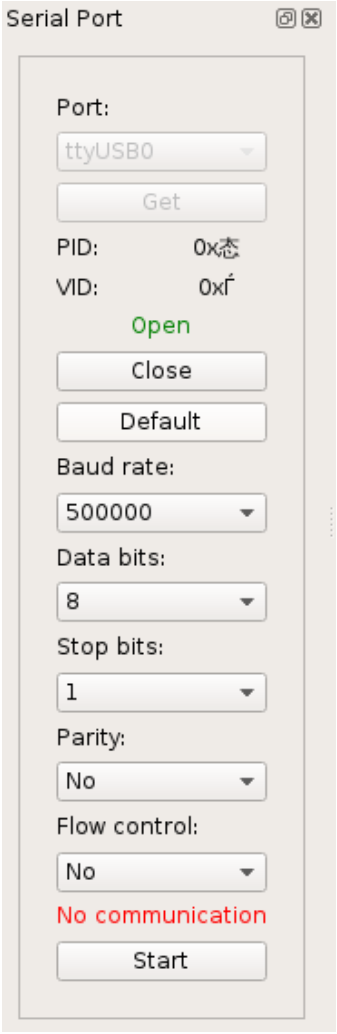
Serial Port
Port:
ttyUSB0
Get
PID:
VID:
Open
Close
Default
Baud rate:
500000
Data bits:
8
Stop bits:
1
Parity:
No
Flow control:
No
No communication
Start

8.2 Logging

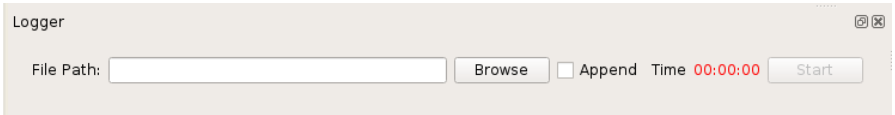

8.3 Live Plotting

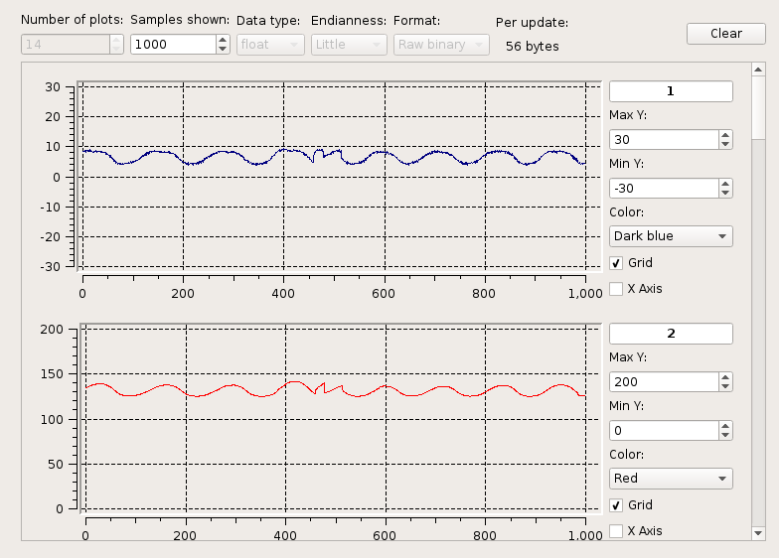

8.4 Control Plug-in

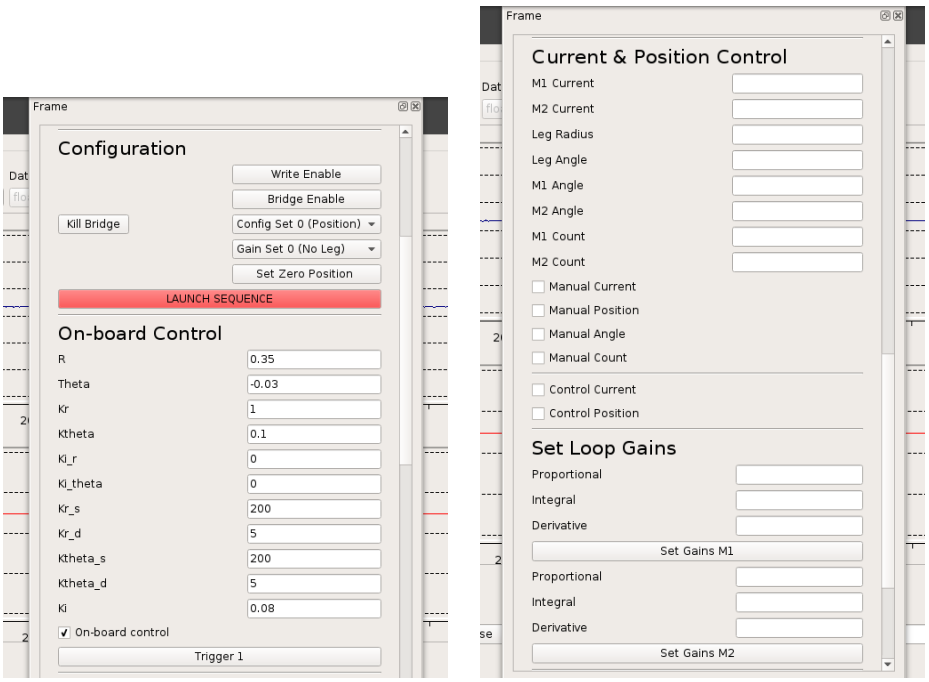

(a) Configuration & On-board Control (b) Current/Position Control & Control Loop Gains

Figure 8.1: Control interface plug-in.

9 Kinematics

Originally derived in [**?**]...

$$f(\phi_1, \phi_2) = \begin{pmatrix} \sqrt{\frac{9}{100} - \frac{9\sin\left(\frac{\phi_1}{2}+\frac{\phi_2}{2}\right)^2}{400}} - \frac{3\cos\left(\frac{\phi_1}{2}+\frac{\phi_2}{2}\right)}{20} & \frac{\phi_1}{2} - \frac{\phi_2}{2} \end{pmatrix} \tag{9.1}$$

$$g(r, \theta) = \begin{pmatrix} \pi - acos(\frac{r^2+l_1^2-l_2^2}{2rl_1}) + \theta \\ \pi - acos(\frac{r^2+l_1^2-l_2^2}{2rl_1}) - \theta \end{pmatrix} \tag{9.2}$$

Taking the Jacobian of the kinematic mapping $f(\phi_1, \phi_2)$ the foot force vector, F, can be transformed to the motor torque commands, τ:

$$J = \left[\frac{\partial \mathbf{f}}{\partial \mathbf{X}}\right] \tag{9.3}$$

where $\mathbf{X}$ = [r θ].

The following force vector provides a constant angular force, f_{theta}:

$$F = [f_r \ f_\theta]^T \tag{9.4}$$

by using f_s, a force related to the arc-length of a polar system, the relation $s = r\theta$ exists:

$$F = [f_r \ f_s]^T \tag{9.5}$$

$$f_a = k_s(a_{fbk} - a_{cmd}) + k_d(\dot{a}_{fbk} - \dot{a}_{cmd}) \tag{9.6}$$

$$\tau = J^T F \tag{9.7}$$

10 Dynamic Modelling

10.1 Robotic Leg Modelling

10.1.1 Virtual Model

Simplicity

10.1.2 Dynamic Model

Complexity

Lagrangian Dynamic Model

In the study [**?**] a Lagrangian model and control system was developed for a hybrid machine system (constant speed motor with servo motor) with a five bar linkage end effector.

10.1.3 SLIP Model

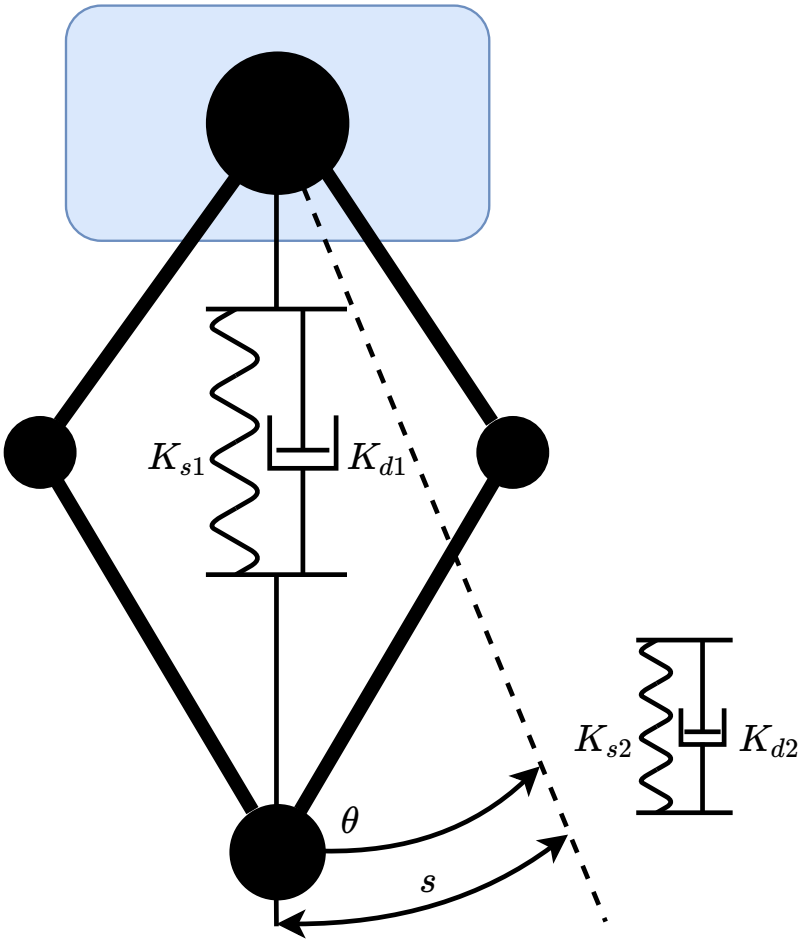

Figure 10.1: Leg spring-damper virtual model.

10.2 Virtual Compliance Model

11 Controller Development

11.1 Active Compliance

Active vs. Passive Compliance

11.2 Dynamic Stability

Static vs. Dynamic Stability

11.3 Mechanical Impedance

Inherent mechanical impedance in the form of friction, slack, inertia, mass.

11.4 Control Loop Sampling Frequency

Limited by motor driver response time...

Figure 11.1 is an adaptation of the control loop design found in [**?**]. Continuous position loop gain scheduling vs virtual spring-damper gain scheduling.

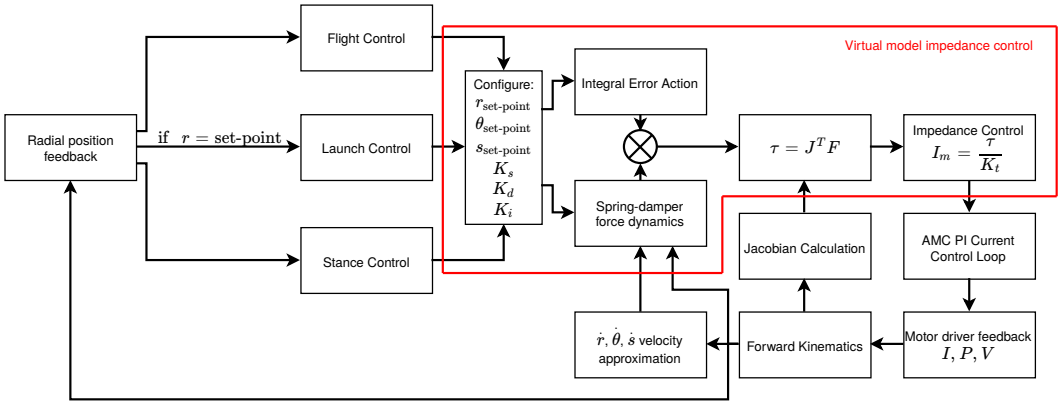

Figure 11.1: Virtual model impedance control loop.

11.5 Current Control for Impulse Launch

Current saturation at 60A.

12 Experimental Testing

"Jump!"

— Van Halen, *1984*

12.1 Virtual Spring-damper Tests

$r_0 = 0.3\ m$
$r_{offset} = r - r_0 = 0.13\ m$

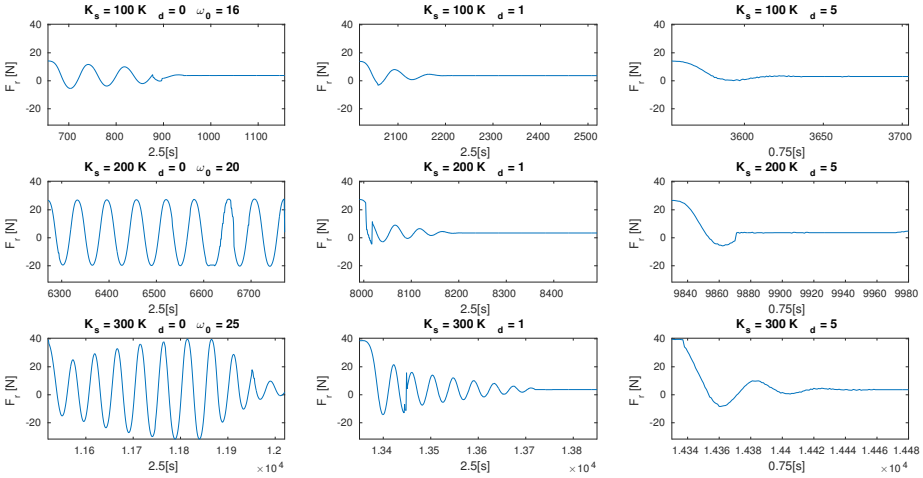

Figure 12.1: Leg spring damper testing for radial offset.

12.2 Drop Tests

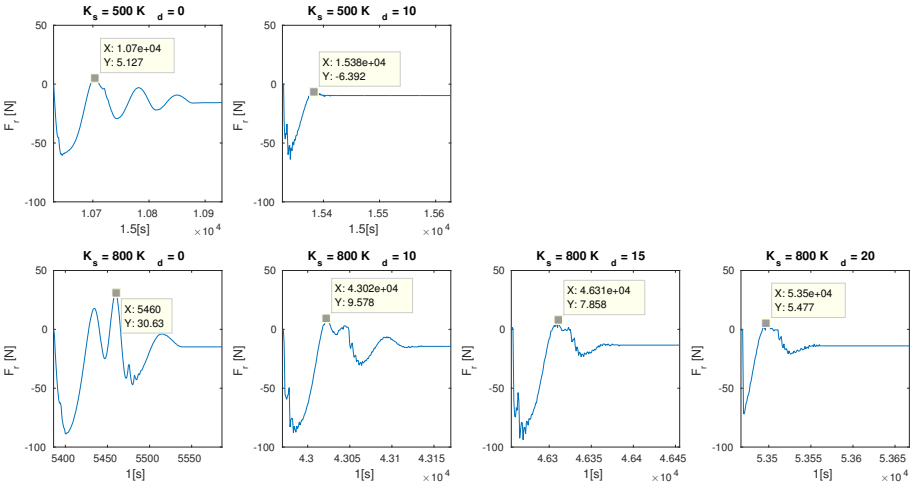

Figure 12.2: Leg spring damper drop testing.

12.3 Launch Tests

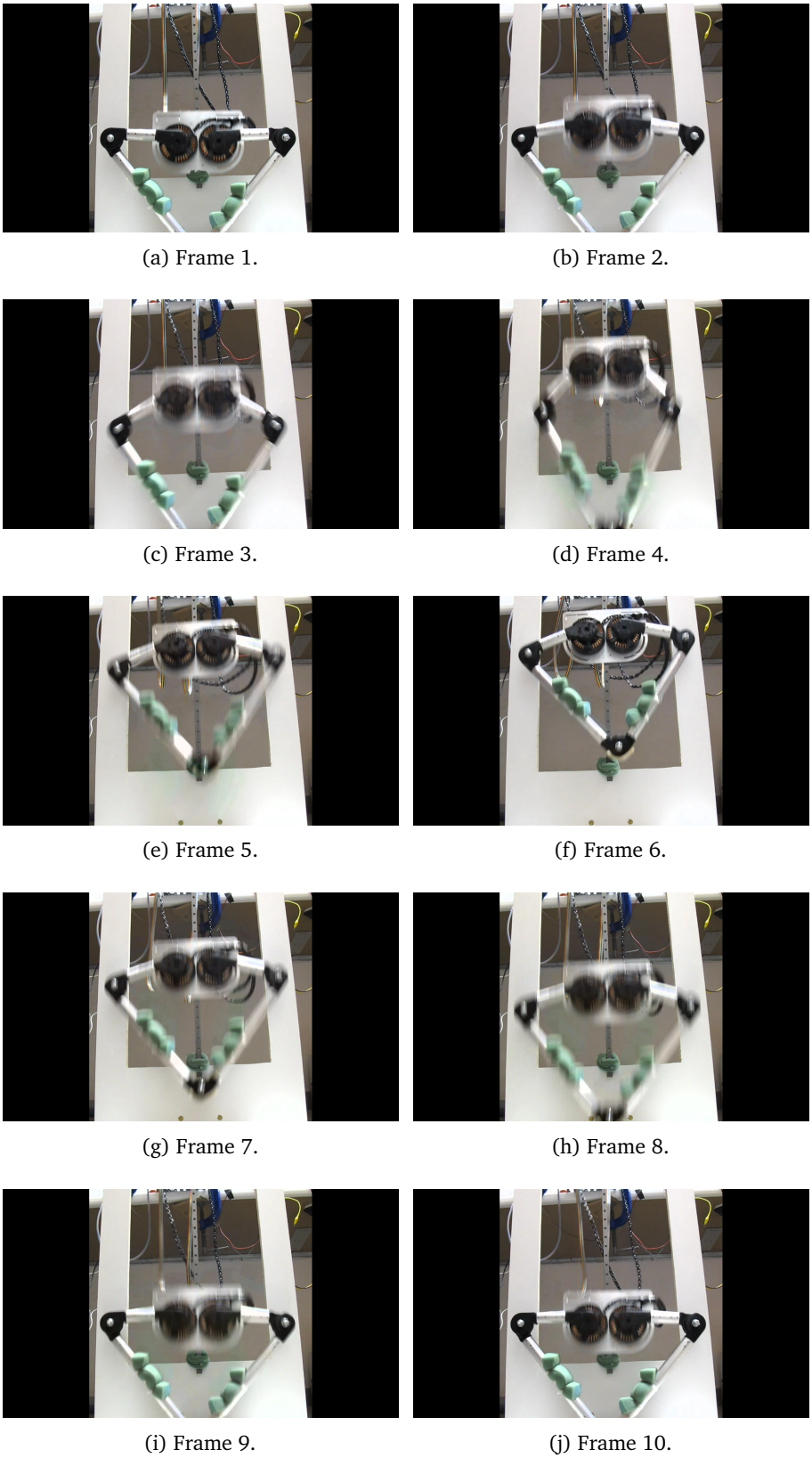

(a) Frame 1. (b) Frame 2.

(c) Frame 3. (d) Frame 4.

(e) Frame 5. (f) Frame 6.

(g) Frame 7. (h) Frame 8.

(i) Frame 9. (j) Frame 10.

Figure 12.3: Leg launch with compliant landing.

13 Design Validation

14 Conclusions

15 Recommendations and Future Work

A Code

Included pieces of code that may not be obvious to users or code that was particularly important to the operation of the protocol.

```
//Communication Timing
uint8_t Ts = 25; //Sampling time in 1/_X_ ms
uint8_t Td = 3;
//NB: #define configTICK_RATE_HZ ((TickType_t)_X_000) in FreeRTOSConfig.h
```

Listing 1: FreeRTOS timing configuration.

```
struct __attribute__((__packed__)) RXPacketStruct {
        uint8_t START[2];
        ...
        uint8_t StatBIT_1 : 1; //Bit field
        uint8_t StatBIT_2 : 1;
        uint8_t StatBIT_3 : 1;
        ...
        uint8_t CRCCheck[2]; //CRC-CCITT
        uint8_t STOP[2];
};
```

Listing 2: PC RX "packed" packet structure.

```
union {
        uint32_t WORD;
        uint16_t HALFWORD;
        uint8_t BYTE[4];
} WORDtoBYTE;
```

Listing 3: Byte conversion union.

```
HAL_UART_Receive_DMA(&PC_UART, RXBufPC, sizeof(RXPacket));
if(xSemaphoreTake( PCRXHandle, portMAX_DELAY ) == pdTRUE) {
        rcvdCount = sizeof(RXPacket);
        START_INDEX = findBytes(RXBufPC, rcvdCount,
        RXPacket.START, 2, 1);
        if(START_INDEX>=0) {
                memcpy(RXPacketPTR, &RXBufPC[START_INDEX],
                sizeof(RXPacket));
                RX_DATA_VALID = 0;

                WORDtoBYTE.BYTE[1] = RXPacket.CRCCheck[0];
                WORDtoBYTE.BYTE[0] = RXPacket.CRCCheck[1];
                CALC_CRC = crcCalc(&RXPacket.OPCODE, 0, PAYLOAD_RX, 0);

                //A useful tool when calculating and
                //confirming CRC values of various types:
                //https://www.lammertbies.nl/comm/info/crc-
                //calculation.html

                if(WORDtoBYTE.HALFWORD==CALC_CRC) {
                        RX_DATA_VALID = 1;
                        ... //Packet processing
```

Listing 4: PC RX packet processing.

```
void BaseCommandCompile(uint8_t n, uint8_t SeqBits, uint8_t ComBits,
uint8_t INDOFF1, uint8_t INDOFF2, uint8_t *DATA,
uint8_t LEN, uint8_t SNIP);
```

Listing 5: Motor packet compilation function.

```
BaseCommandPTR = &BaseCommand[RXPacket.OPCODE];
BaseCommandCompile(RXPacket.OPCODE, 0b0011, 0x02, 0x45, 0x02,
RXPacket.M1C, 2, 0);
xQueueOverwrite(ICommandM1QHandle, &BaseCommandPTR);
```

Listing 6: Motor packet compilation current command example.